J. Fluid Mech. (1980), *vol.* 96, *part* 4, *pp.* 641–669
Printed in Great Britain

Evolution of a spectrally local disturbance in grid-generated, nearly isotropic turbulence

By R. M. KELLOGG
IBM Corporation, Endicott, New York 13760
AND S. CORRSIN
The Johns Hopkins University, Baltimore, Maryland 21218

(Received 20 June 1978 and in revised form 15 June 1979)

A grid-generated 'isotropic' turbulent flow has been subjected to a spectrally local perturbation in the form of a high wavenumber, sinusoidal ripple in the mean velocity. It is introduced as the wake of a fine wire, low solidity screen (a 'zither'), operating below its vortex-shedding Reynolds numbers. The perturbation appears most clearly downstream as a strongly periodic component in the transverse correlation of streamwise turbulent velocity, $R_{11}(r_2)$. Its Fourier transform, $E_{11}(k_2)$, a 'one-dimensional spectrum', shows a corresponding local 'spike'. The downstream evolution of this perturbation has been chronicled for four different spectral locations. Their decays are approximately exponential. Measurements of the one-dimensional spectrum $E_{11}(k_1)$ at several downstream stations show evidence of energy transfer to other wavenumber regions.

The decay of the velocity correlation ripple is approximately consistent with the decrease in time of the narrow-band correlation function presented by Comte-Bellot & Corrsin (1971). It is also found that the linear perturbation response calculated by Kraichnan (1959) for a disturbance wavenumber larger than those of the incident turbulence shows fair agreement with this decay.

1. Introduction

Dynamical systems are often studied both experimentally and theoretically by their responses to appropriate perturbations. In fluid mechanics experiments, the best-known early example may be the Schubauer & Skramstad (1947) measurement of the laminar boundary-layer response to controlled periodic perturbation introduced by a thin vibrating ribbon.

In turbulence research, the first explicit work on a perturbation was Lin's (1951) theoretical estimate of the initial decay rate of a small spectral spike. He applied the Heisenberg formula for spectral transfer, and was interested in the stability of the similarity spectrum. Liepmann (private communication *c.* 1952) and Roshko (1953) suggested that relevant basic information could be extracted if a fully developed turbulent flow were disturbed by a periodic velocity field.

The present experiment was motivated primarily by Kraichnan's (1959) introduction to turbulence theory of the notion of a spectral response tensor, a sort of 'Green's function' of a fully-developed field of turbulence. It can be thought of as a more integrated and sophisticated version of Lin's perturbation because no initial spectrum

0022–1120/80/4376–8280 $02.00

is assumed; the spectral function and response function are simultaneous unknown functions.

Townend's (1956) analysis of a fully turbulent, periodic wake flow has some relevance to the present work. He treats a field of homogeneous turbulence subjected to a small velocity perturbation. By neglecting terms in the square of the perturbation, and restricting attention to the case where the scale of the perturbation is large compared with that of the important turbulence structure, he argues that the equation of motion for the perturbation velocities may be approximated by an equation of the same form as the heat-conduction equation. By analogy to the experimental results for a point source of heat in isotropic turbulence, he then obtains an exponential decay for the periodic wakes.

2. Experimental design

The basic turbulence to be disturbed was 'standard', decaying, nearly-isotropic turbulence generated by moderate-solidity, bi-plane, square rod grid spanning a low turbulence level, uniform air flow in a straight duct, which diverged slightly to compensate for the growth of the wall boundary layers. A fairly complete summary of these flows is included in a paper of Comte-Bellot & Corrsin (1966).

The spectral disturbance of greatest simplicity for theoretical study might be statistically isotropic, very weak, and at a single wavenumber magnitude, i.e. a thin, weak, spherical shell in wavenumber space. We have not yet devised a method for generating such an ideal disturbance.

A more rudimentary spectral disturbance, which is certainly easier to generate experimentally, is one which is local in the one-dimensional spectrum and hence is contained in a thin, plane slab in wavenumber space (see, for example, Corrsin 1959). This implies a velocity disturbance which is a single, simple sinusoid in the physical space.

The requirement that the perturbation energy be much less than the pre-existing total turbulent energy turns out to be difficult to satisfy. Further discussion of this difficulty will be given later.

To remain within the realm of an incompressible turbulent flow, the perturbation must be solenoidal. This rules out acoustically generated perturbations.

Finally, it should be most relevant to focus this study initially on the wavenumber range between the region of primary energy content (the inverse of the integral scale) and the dissipation region, characterized by the inverse of the Kolmogorov microscale. This is the region which has both important Fourier mode dynamic interactions and some degree of universality. Eventually, disturbances at both larger (viscous) and smaller wavenumbers should be studied.

The methods considered for introducing a perturbation which would satisfy most of the above requirements were:

(*a*) vortex shedding from a plane array of parallel circular cylinders normal to the mean flow;

(*b*) an array of parallel cylinders (possibly of airfoil shape) at low Reynolds number, forced to oscillate in a plane normal to the direction of the mean flow, or to change their angles of attack periodically;

(*c*) an array of stationary parallel cylinders at low Reynolds number, leaving 'laminar wakes';

(*d*) a modification of the turbulence-generating grid itself, perhaps the use of rotating elliptic or prismatic rods, which would add a periodic disturbance to the grid solidity.

The first three of these methods were investigated sufficiently to assess their advantages and limitations. The devices with vortex shedding from fixed wires, and with oscillating circular cylinders, created disturbance periodic in two space directions and time. The small Reynolds number round-wire array created a disturbance which was periodic solely in one direction of space. Therefore this last method was selected because the disturbance introduced was the simplest, and the amount of new fluctuation energy introduced was the smallest of the methods investigated, although larger than desired.

The perturbing array of parallel circular cylinders was in fact a screen of taut parallel wires, called for obvious reasons the 'zither'. Its dimensions were as follows: wire diameter $d = 0{\cdot}003$ in.; wire spacing $m = 0{\cdot}064$ in. on centres; solidity $\sigma = 0{\cdot}047$; wire Reynolds number $R_w \equiv \overline{U}^{\tau} d/\nu = 25$. $\overline{U}^{\tau}$ is the mean velocity away from the zither plane.

The wire tension was adjusted to keep the wires from bowing significantly due to aerodynamic drag. Neither observation with a long focal length microscope, nor frequency analysis of a hot-wire signal taken directly behind one of the wires showed any wire vibration.

The decisions on wire spacing and diameter were a compromise. An upper limit on the wire Reynolds number avoided periodic vortex shedding; a lower limit on the wire diameter provided strength and ease of fabrication; an upper limit on the grid mesh size was set by the tunnel cross-section. The air speed could not be reduced too far because a large grid Reynolds number was desirable.

The individual laminar wakes were initially separated by a distance considerably larger than their characteristic widths. But they spread and their mean velocity deficiencies decayed, so that they became a simple sinusoidal mean velocity perturbation spanning the turbulence field.

Since grids were easier to construct than zithers, the change in *relative* wavenumber of the perturbation was achieved by employing grids of differing mesh size placed in turn upstream of the single zither.

3. Equipment

The wind tunnel (figure 1) was basically that used by D. S. Johnson (1957). It has a 12 in. by 18 in. test section and was modified by the addition of a closed return, the introduction of filters, the mounting of pockets to hold the zither and grids, and the addition of access ports.

The four pockets were mounted so that the sequential spacing between them was 34 in., 20 in. and 20 in. The zither was always at the farthest downstream location. This arrangement allowed the grid mesh size to be varied while the number of mesh lengths between the zither and grid was kept essentially constant.

The free-stream turbulence level measured at the zither location was $0{\cdot}1\%$ for a mean speed of 16 ft/s.

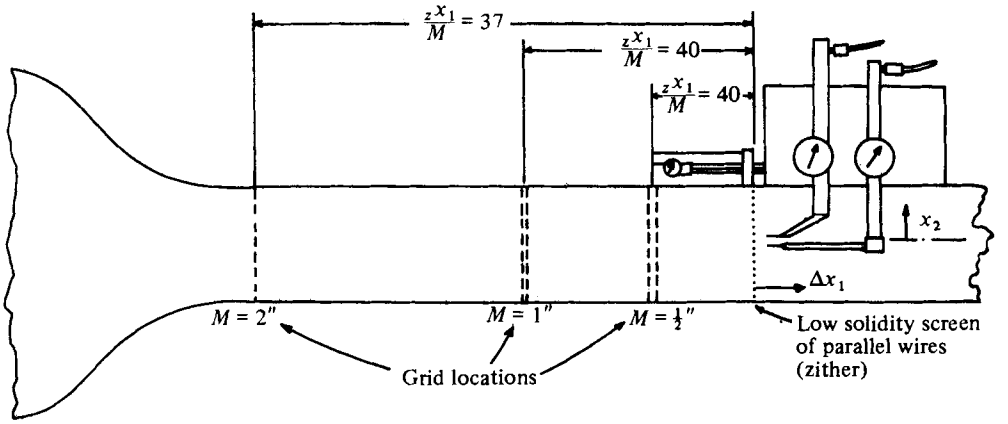

FIGURE 1. Wind tunnel arrangements.

The grids used were of square rod, square mesh, bi-plane construction. The mesh sizes were 2·0, 1·0 and 0·50 in. and the solidities were all 0·30. The 2 and 1 in. mesh grids were made from brass rod pinned at alternate intersections. The 0·5 in. grid was made by gluing together two sheets of mahogany with their grain directions perpendicular, then machining out the unwanted parts of each sheet, parallel to its grain.

Turbulence uniformity check traverses were taken at $x_1/M = 40$ (37 for the 2-inch grid). These indicated that u_1' was uniform over x_2 to within $\pm 0{\cdot}5\%$ over the central portion of the tunnel for the two larger grids. The wooden grid was less accurate; its u_1' non-uniformity was $\pm 3{\cdot}0\%$.

The traversing mechanism moved the probes in steps as small as 0·004 in., with an accuracy an order of magnitude smaller than this.

Two different constant-current hot-wire anemometers were used. Figure 2 shows schematically one channel used for the measurement of the u_1' levels, the mean profiles, the two-point velocity correlation coefficients $R_{11}(r_2)$ and the one-dimensional spectra. The battery-operated amplifiers were operated with 3 dB points at 40 kHz for the high frequency end, and at 0·2 Hz for the low frequency end.

The measurements of the two-point velocity correlation coefficient $R_{33}(r_2)$ and the u_2' levels were made with a Shapiro–Edwards constant-current hot-wire set. The band-pass for these measurements was set with 3 dB points at 20 kHz and 1 Hz.

All measurements were taken with hot wires made from platinum/10% rhodium Wollaston wire. The wire diameter was 0·0001 in. for all but the spectral measurement. There it was 0·00005 in. Wire lengths were approximately 0·03 in.

The instruments used were the following: for determining the fluctuation level, a Ballentine Model 320 true r.m.s. electronic voltmeter; for the one-dimensional spectra, a Hewlett–Packard Model 302A wave analyser. The analyser was modified so that the 100 kHz I.F. signal was available as an output, its amplitude being proportional to the energy at the frequency selected. The mean square level was obtained with the Ballentine r.m.s. meter, integrating its mean square output with a Texas Research and Electronic Co. Model SI-100 integrator. The integrator output, a d.c. voltage, was read with a Cubic Corporation Model V46-P digital voltmeter.

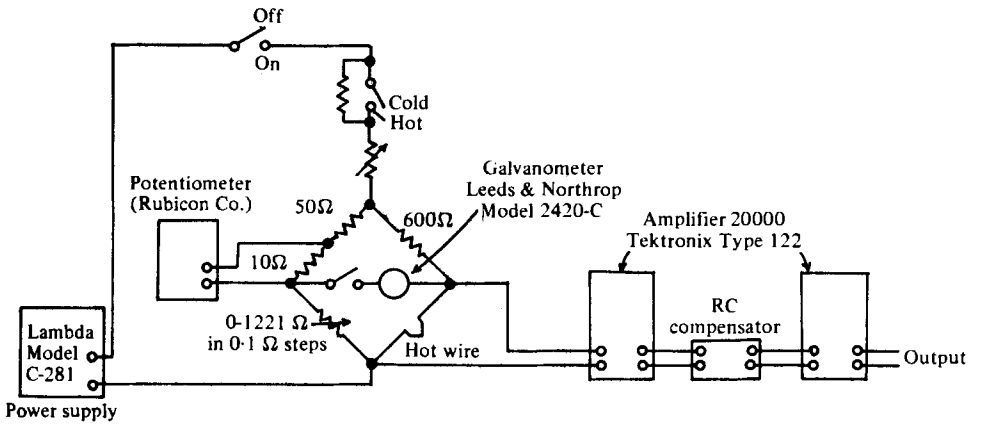

FIGURE 2. Hot-wire anemometer schematic circuit.

The correlations were measured by the mean sum and difference of the square voltages (the 'quarter square' method). The instantaneous sum and difference were obtained by conventional operational amplifier techniques. The units used were a Philbrick Model K-2-XA for the sum and a Philbrick Model SK2-V for the difference. The mean square level was obtained by the Ballantine integrator/digital voltmeter combination.

The tunnel air temperature was measured by a Veco number 31A2 thermistor resistance thermometer.

4. Results of measurements

The unperturbed turbulence fields generated by the three test grids were statistically in good agreement with more extensive experiments, especially those of Comte-Bellot & Corrsin (1966, 1971) behind square-rod, square-mesh, bi-plane grids, so the details need not be given here. The small differences are attributable to the smaller grid Reynolds numbers here, and to the slightly smaller grid solidities.

Table 1 summarizes the simplest turbulence properties at the zither location and includes the ratios of the zither mesh size to the transverse integral scale and the Kolmogorov microscale. The latter scales were estimated from the dissipation rates given by the turbulent energy decay.

L is the 'transverse' integral scale, η the Kolmogorov microscale, ν the kinematic

Grid mesh M (in.)	$\bar{U}M/\nu \equiv R_M$	x_1/M	L (in.)	$u_1'/\bar{U}$	$u_1'L/\nu \equiv R_L$	$u_1'\lambda/\nu \equiv R_\lambda$	$\eta \times 10^3$ (in.)	m/L	m/η
2	16520	37	0·47	0·021	81·3	46·9	2·2	0·14	29·1
1	8260	40	0·22	0·020	36·4	31·3	2·8	0·29	22·9
½	4130	40	0·11	0·022	20·0	23·0	3·4	0·58	18·8
1	8260	77	0·29	0·013	31·1	29·0	4·1	0·22	15·6

TABLE 1. The value of R_η is estimated

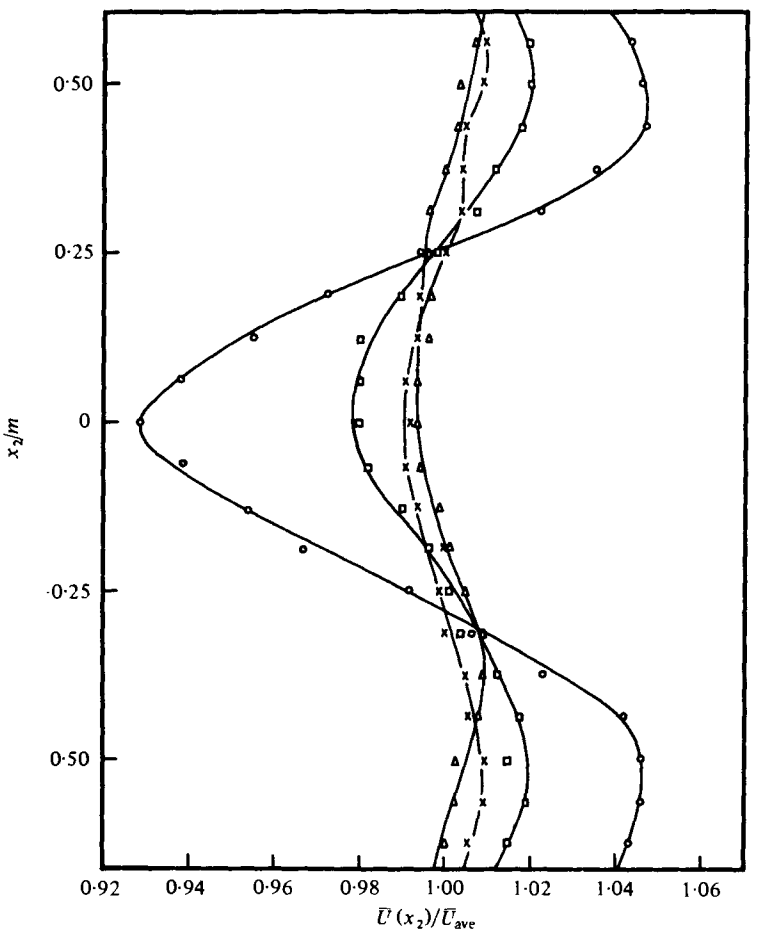

FIGURE 3. Mean velocity profiles behind zither with 2 in. grid and ${}_gx_1 = 37M$. Values of $\Delta x_1/d$: ○, 100; □, 200; ×, 250; △, 300.

viscosity, λ the transverse Taylor microscale and m the zither mesh size. ${}_gx_1$ is the downstream distance from the grid to the zither.

L is the 'transverse' integral scale, η is the Kolmogorov microscale, ν the kinematic viscosity, λ the transverse Taylor microscale and m the zither mesh size. ${}_gx_1$ is the downstream distance from the grid to the zither. We see that in all cases the zither mesh was appreciably smaller than the transverse integral scale and larger than the Kolmogorov microscale.

Figures 3 and 4 show, over one lateral wavelength, the downstream development of the mean velocity profile behind the zither for $M = 2$ in., ${}_gx_1 = 37M$. Since the intent was to have, within the turbulence, an approximately sinusoidal mean speed variation at $\Delta x_1 = 100d$, the figure 3 data show reasonable success. The decays of the mean disturbances in the two cases shown in figure 5 are both virtually exponential for $\Delta x_1 \gg d$. This is expected from laminar flow theory for the no-grid, laminar wakes, but is surprising for the turbulent case.

Δx_1 is the downstream distance from the zither, x_2 is the transverse distance normal

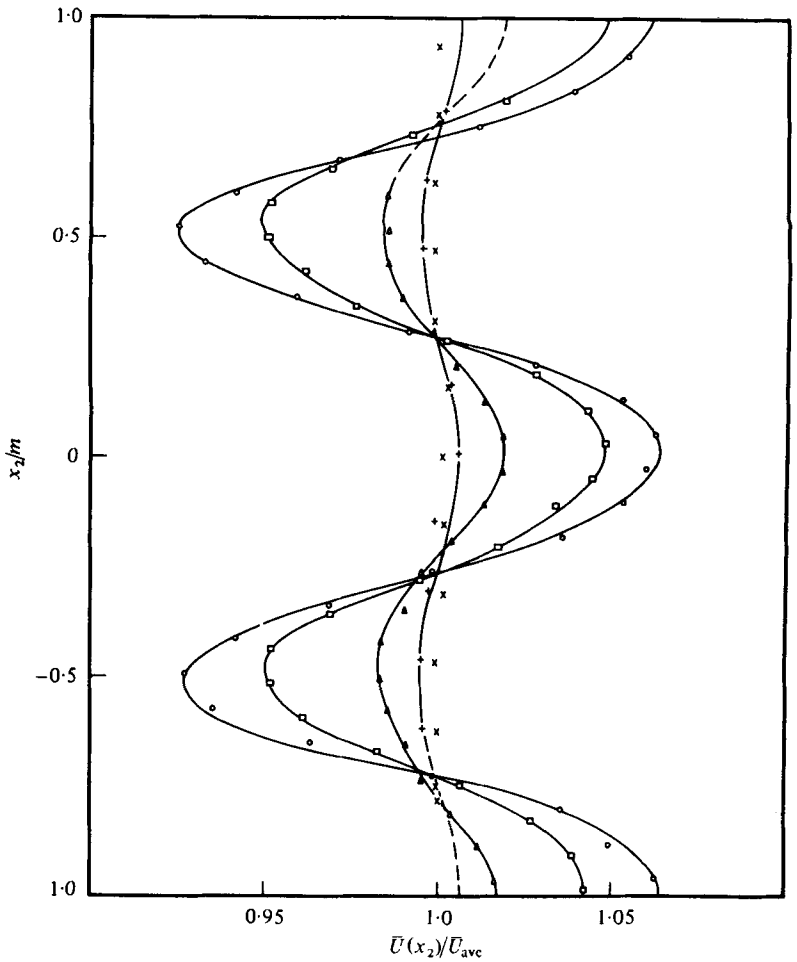

FIGURE 4. Mean velocity profile behind zither with no grid. Values of $\Delta x_1/d$: ○, 200; □, 300; △, 600; +, 900; ×, 1200.

to the wires and x_3 is the transverse distance parallel to the wires. Later in this paper, where two-point correlation functions are presented, r_1, r_2 and r_3 are separation distances along the x_1, x_2 and x_3 axes respectively. k_1, k_2, k_3 are the corresponding wavenumber components.

The decay in mean disturbance amplitude in the turbulent case can be viewed as a kind of spectral relaxation, one reason for the invention of this experiment. On the other hand, the concomitant turbulence inhomogeneity (figure 6) clouds this interpretation a bit.

The laminar and turbulent exponential decays in figure 5 can be represented approximately by

$$\bar{U}_1(x_1, x_2) \approx \bar{U}\left\{1 - \frac{B}{2}\cos\left(\frac{2\pi x_2}{m}\right)\exp\left(-\beta\frac{\Delta x_1}{d}\right)\right\}, \tag{1}$$

where B is the hypothetical peak-to-peak amplitude at $\Delta x_1 = 0$, obtained by backward extrapolation:

$$B \equiv \bar{U}^{-1}[\bar{U}_1^{\max}(0) - \bar{U}_1^{\min}(0)].$$

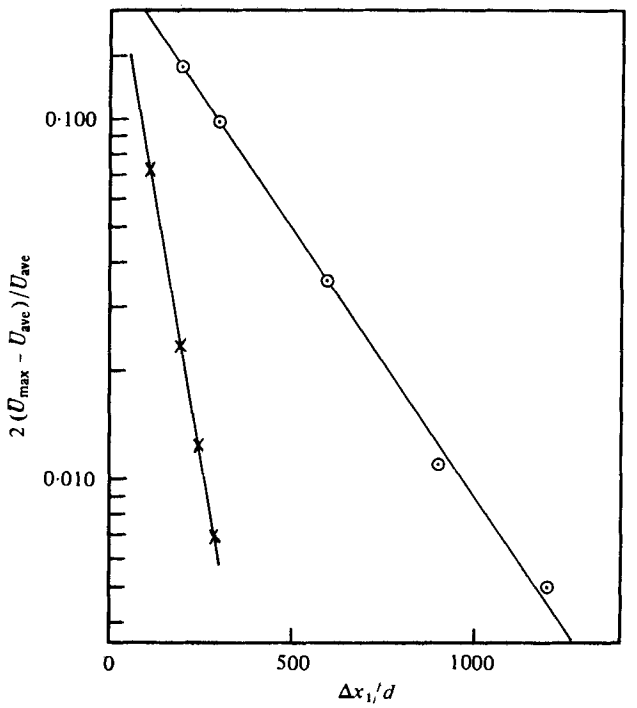

FIGURE 5. Decay of mean velocity profile amplitude behind zither: ⊙, without grid; ×, with grid (M = 2 in., ${}_gx_1 = 37M$).

$\overline{U}$ is the area mean value of $\overline{U}_1$. The dimensionless decay rates for the lines in figure 5 are $\beta_{lam} = 0{\cdot}0034$ and $\beta_{turb} = 0{\cdot}012$. The decay rate measured for the laminar case, transformed to an inverse time, agrees within 3% with $2\pi\nu/m^2$, the laminar theoretical value for a simple sinusoidal flow. If we introduce the concept of an eddy viscosity ν_T to formulate a rough estimate of the turbulent case (Townsend 1956, pp. 56–63), a brief calculation shows that

$$\nu_T/\nu = \beta_{turb}/\beta_{lam} = 3{\cdot}5.$$

This is a remarkably small ratio; in similar turbulence, ratios of turbulent to molecular thermal diffusivity (Uberoi & Corrsin 1953; Wiskind 1962) have been estimated at 15 to 50. Even more contrast is offered by Stewart's (1952) estimate of $\nu_T/\nu \approx 167$ in the decay of the mean velocity variation behind a parallel-rod, turbulence-generating grid.

The difference between Stewart's ratio and the present one is presumably a reflexion of the considerable difference in the ratio of the mean flow wavelength to the turbulence integral scale for the two cases. In his case it was of order one; here it is of order 0·03.

Figure 6 shows the downstream development of the $u_1'/\overline{U}$ turbulence level profile behind the zither for M = 2 in., ${}_gx_1/M = 37$. The most obvious effect is the large increase in level close to the zither, compared with the level upstream. The maxima occur at approximately the same x_2/m locations as the points of maximum mean shear for the mean speed profiles. This, together with the relative minimum on the cylinder

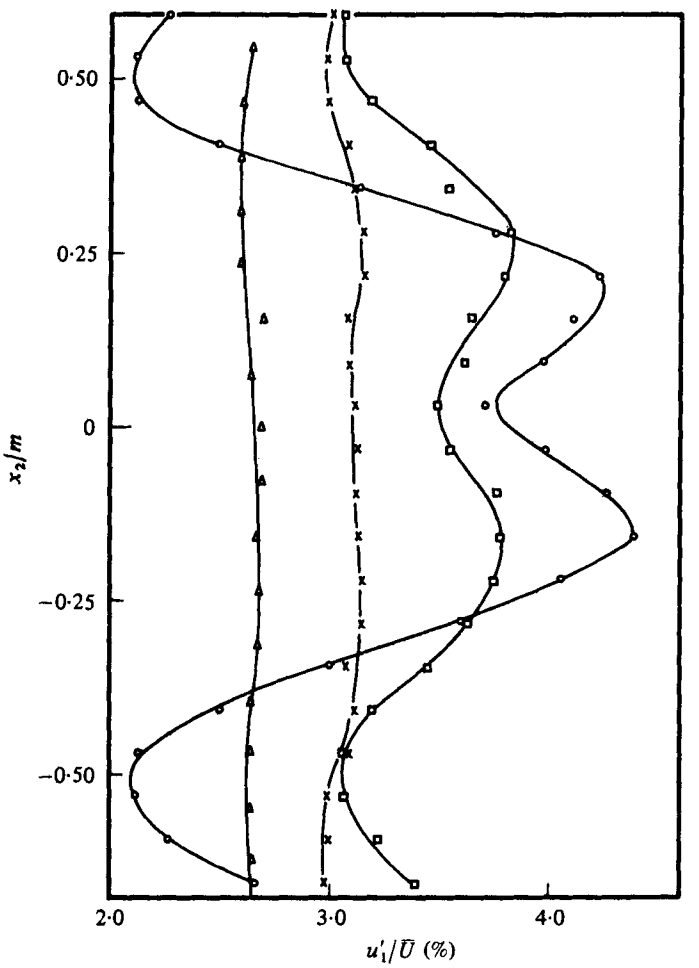

FIGURE 6. $u_1'/\bar{U}$ profiles behind zither with 2 in. grid and $x_1 = 37M$.
Values of $\Delta x_1/d$: ○, 100; □, 200; ×, 250; △, 300.

axis, bears a striking resemblance to corresponding measurements in a single, plane turbulent wake (Townsend 1949). This resemblance suggests that this increased level is the result of turbulent energy production by a local Reynolds stress $-\overline{u_1 u_2}$ acting on the mean shear.

Direct experimental investigation of this suggestion would have been difficult because of the small physical scale of the disturbance; a typical 'small' probe (i.e. X-meter or inclined wire) would have been the same size as the disturbance. For this reason no attempt at measuring $\overline{u_1 u_2}$ was made. However, a rough theoretical estimate can be made by using as an approximation the value of $\overline{u_1 u_2}$ obtained in an ordinary wake. This is presented in the following section.

Figure 7 shows the $u_1'/\bar{U}$ decay 'far' downstream of the zither, for $M = 2$ inches. Included also are a few values of $u_2'/\bar{U}$. The values indicated at $\Delta x_1/d = 0$ are the incident levels. The decay of $u_1'/\bar{U}$ without the zither, given by the dashed line, is

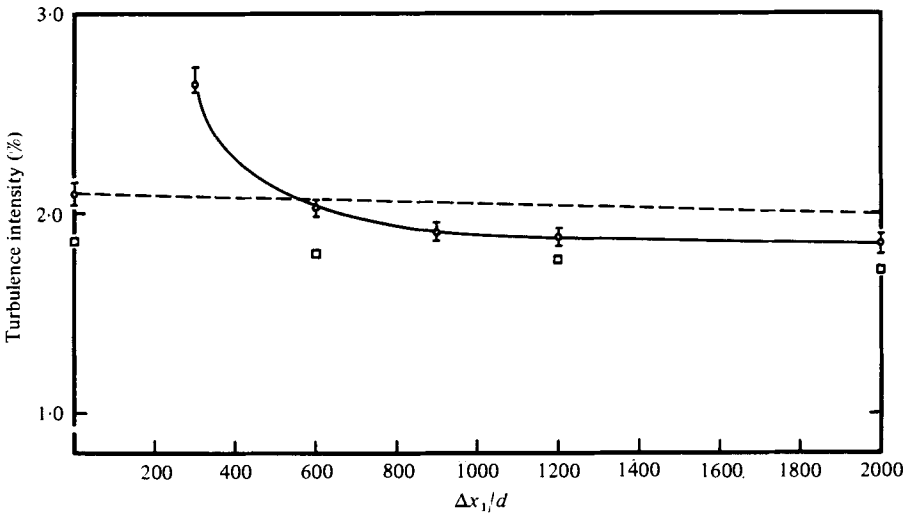

FIGURE 7. $u_1'/\overline{U}$ and $u_2'/\overline{U}$ decay far downstream of zither with 2 in. grid, ${}_sx_1 = 37M$. ○, $u_1'/\overline{U}$; □, $u_2'/\overline{U}$.

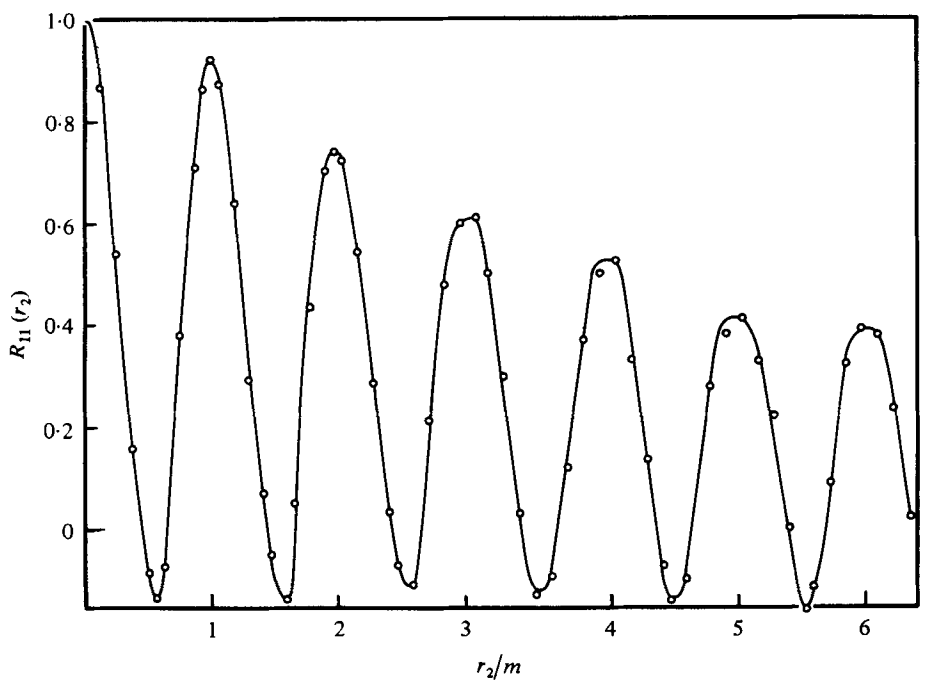

FIGURE 8. Correlation function $R_{11}(r_2)$ behind zither at $\Delta x_1/d = 100$. $M = 2$ in.; ${}_sx_1 = 37M$.

included for reference. The decay of $u_1'/\overline{U}$ from its increased level close to the zither is more rapid than the decay of unperturbed grid turbulence. Furthermore, the $u_1'/\overline{U}$ levels 'far' downstream ($\Delta x_1/d > 600$) are lower than those expected for the decay of grid turbulence. This is consistent with the known action of damping screens

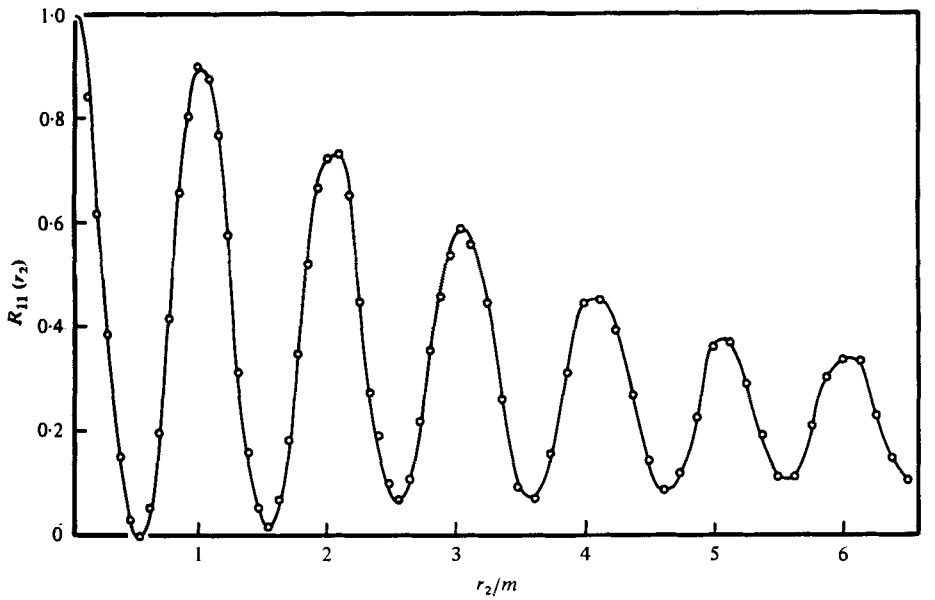

FIGURE 9. $R_{11}(r_2)$ behind zither at $\Delta x_1/d = 300$. $M = 2$ in.; $_{s}x_1 = 37M$.

on 'wind tunnel' turbulence (Schubauer, Spangenberg & Klebanoff 1950; Townsend 1951*a*). Direct comparison of these data with those far behind 'damping screens' are difficult because of the relatively low solidity, and hence small pressure drop coefficient $[\Delta p/(\frac{1}{2}\rho\overline{U}^2) = 0{\cdot}06$ for $\overline{U} = 16$ ft/s] of the zither.

The typical effect of the zither on the two-point velocity correlation $R_{11}(r_2)$ is shown in figures 8, 9, and 10. The numerical data, which extend to much larger r_2/m, are tabulated by Kellogg (1965). The reference correlation function without the perturbation is in figure 11. These data clearly show the sinusoidal nature of the perturbation. The strength of this correlation function ripple is perhaps a little surprising, not so much for $\Delta x_1/d = 100$ (figure 8), where large inhomogeneities in the $\overline{U}_1$ and $u_1'/\overline{U}$ profiles exist, but rather at $\Delta x_1/d = 300$ (figure 9), where these profiles are uniform in x_2. Why this should be the case is not certain, but the following speculation can account for this behaviour.

At $\Delta x_1/d = 300$, equation (15) in the following section predicts a material point r.m.s. lateral dispersion of $(\overline{X_2^2})^{\frac{1}{2}} = 18 \times 10^{-3}$ in. Presumably peak-to-peak excursions of three times this value occur. In any case, the turbulence-induced lateral displacement is of the same order as the zither mesh size. Assuming then that a closely sinusoidal variation in the 'instantaneous laminar mean velocity' still existed, the fact that this disturbance was being convected laterally past the point of measurement on a scale of the same order as the wavelength of the disturbance could account for the virtual uniformity of the mean velocity profile. A two-point correlation measurement, however, would easily detect the regularity in such a randomly flapping profile. The total correlation measured would then be the sum of a part due to the randomly convected, periodic laminar wakes and a part due to the original correlation of the incident turbulence itself. The contribution from the laminar wakes would be either

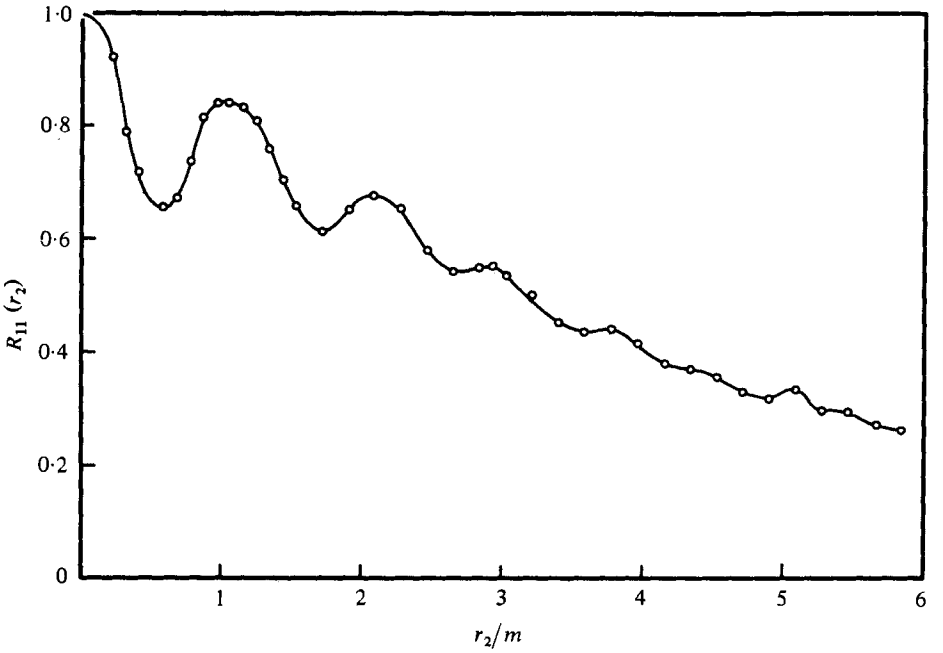

FIGURE 10. $R_{11}(r_2)$ behind zither at $\Delta x_1/d = 600$. $M = 2$ in.; ${}_sx_1 = 37M$.

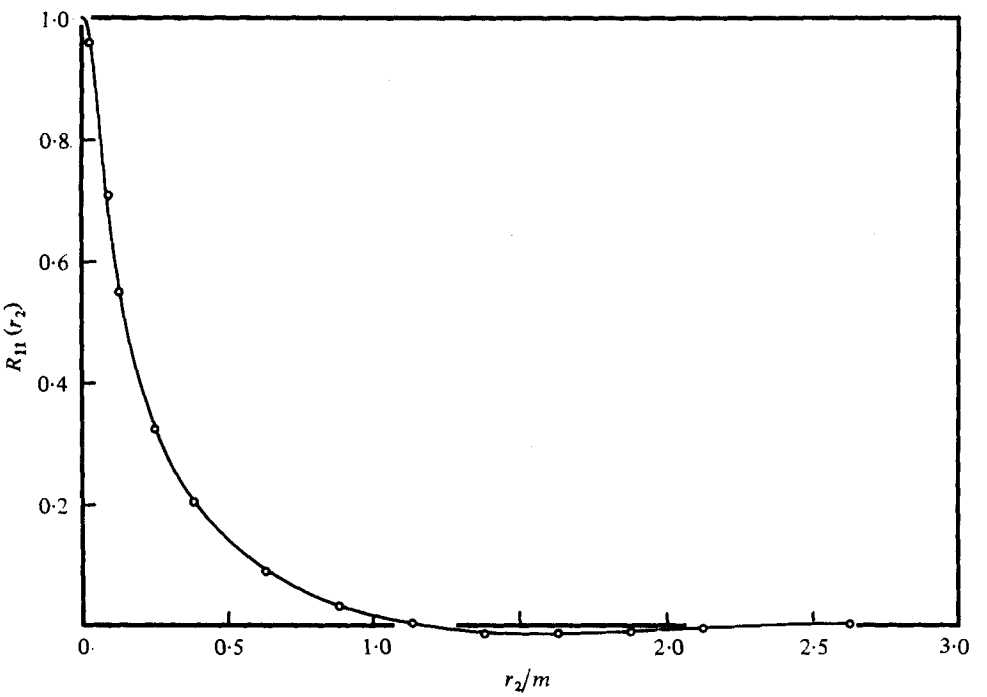

FIGURE 11. $R_{11}(r_2)$ without zither. $M = 2$ in.; $x_1/M = 37$.

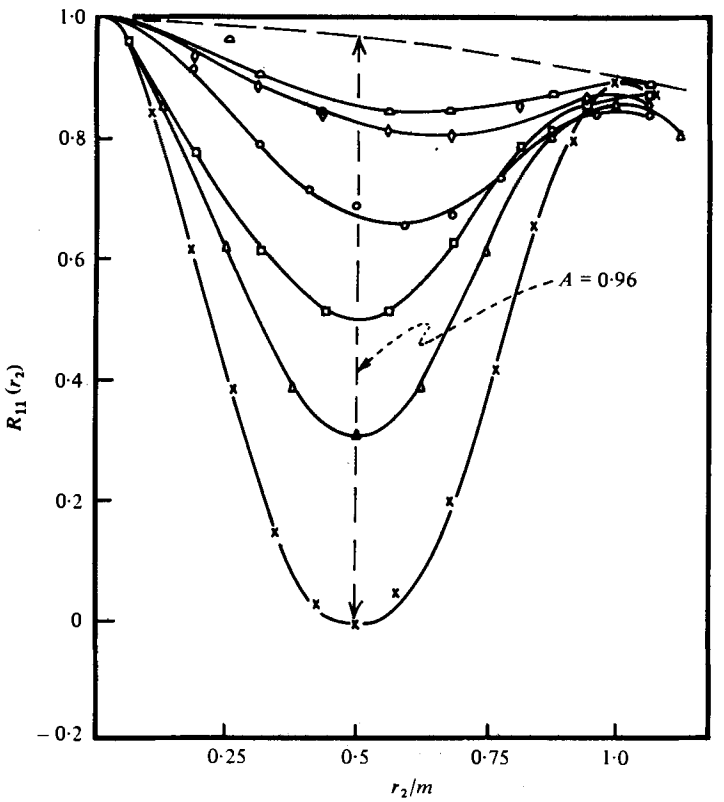

FIGURE 12. Downstream development of first cycle of correlation function ripple. $M = 2$ in.; $\Delta x_1/M = 37$. Values of $\Delta x_1/d$: ×, 300; △, 400; □, 500; ○, 600; ◇, 700; ⌓, 800.

positive or negative, depending on the relation between the separation distance of the hot-wire probes and the wavelength of the disturbance.

The effect of changing the grid mesh size, while keeping the number of grid mesh lengths between the grid and zither essentially constant (Kellogg 1965), is a more rapid fall of $R_{11}(r_2)$ as a function of r_2/m behind the finer grid. This is because of the smaller transverse integral scale of the incident turbulence. Being closer in size to the laminar wake spacing, it 'scrambles' the periodic structure more effectively.

One simple measure of the amount of ripple in $R_{11}(r_2)$ is the depth of the first dip (at $r_2/m = 0{\cdot}5$). The downstream decrease in this dip is a measure of the relaxation of the perturbation. A typical set of data for this effect is presented in figure 12, for the case of $M = 2$ inches, $_{\varepsilon}x_1/M = 37$.

The downstream decays of the first dip amplitudes A for the four cases studied are summarized in figure 13. A was arbitrarily chosen to be the maximum difference between the measured correlation function and a parabola drawn through the vertex and tangent to the first peak, near $r_2/m = 1$. Evidently the perturbation history changes with changes in energy and relative scale of the incident turbulence.

The 'early' strengths (A at $\Delta x_1/d = 300$) of the perturbations in the four cases are listed in table 2. By inspection we see that $A(300)$ is not monotonic with L (or L^{-1}),

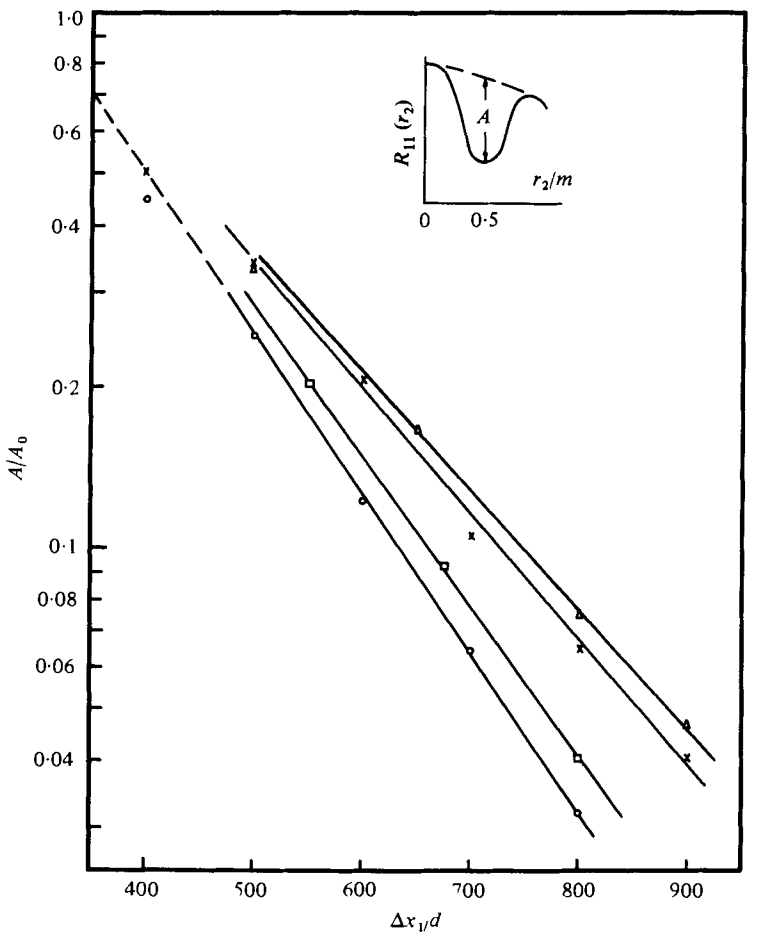

FIGURE 13. Decay of amplitude of first cycle of correlation function ripple. [M (in.), x_1/M, incident $u_1'/\bar{U}$ (%)]: ○, ($\frac{1}{2}$, 40, 2·2); □, (1, 40, 2·0); ×, (2, 37, 2·1); △, (1, 74, 1·3).

but is monotonic with $(u_1')^{-1}$. This latter fact seems to support the speculation made previously that the correlation can be considered as the sum of a part due to the incident turbulence and a part due to the lateral random convection of a 'fixed' periodic wake structure.

The exponential decay rates of A (figure 13) were estimated as follows. The effects of the different incident energy levels were removed by scaling the amplitudes: a semi-log plot of each amplitude A against $\Delta x_1/d$ was made. It was easily fitted with a straight line in all cases. The linear portion was extrapolated backward to a hypothetical value at $\Delta x_1/d = 300$. Designated 'A_0', this value was used to normalize A. In effect, the decay data were fitted with lines having the form

$$A/A_0 = \exp\left[-\alpha(d/\bar{U})\,(\Delta x_1/d)\right] \tag{2}$$

for $\Delta x_1/d \geqslant 500$. The (exponential) decay rates α obtained in this fashion are included in table 2. For easy comparison, two 'rates' in the incident turbulence are also tabulated: u_1'/L is proportional to the turbulent energy decay rate (and is a sort of 'big

Case: Grid mesh M (in.)	Case: Zither location $_sx_1/M$	Incident turbulence: $\sim$ (scale)$^{-1}$ m/L	Incident turbulence: Level u_1'/U %	First dip in $R_{11}(r_2)$ at $\Delta x_1/m = 300$: A	Exponential decay rate of A/A_0: α (s^{-1})	u_1'/L (s^{-1})	u_1'/λ (s^{-1})
2	37	0·14	2·1	0·96	347	8·6	14·9
1	40	0·29	2·0	1·08	411	17·4	20·2
½	40	0·58	2·2	0·81	444	37·4	32·5
1	77	0·22	1·3	1·34	324	8·7	9·3

TABLE 2

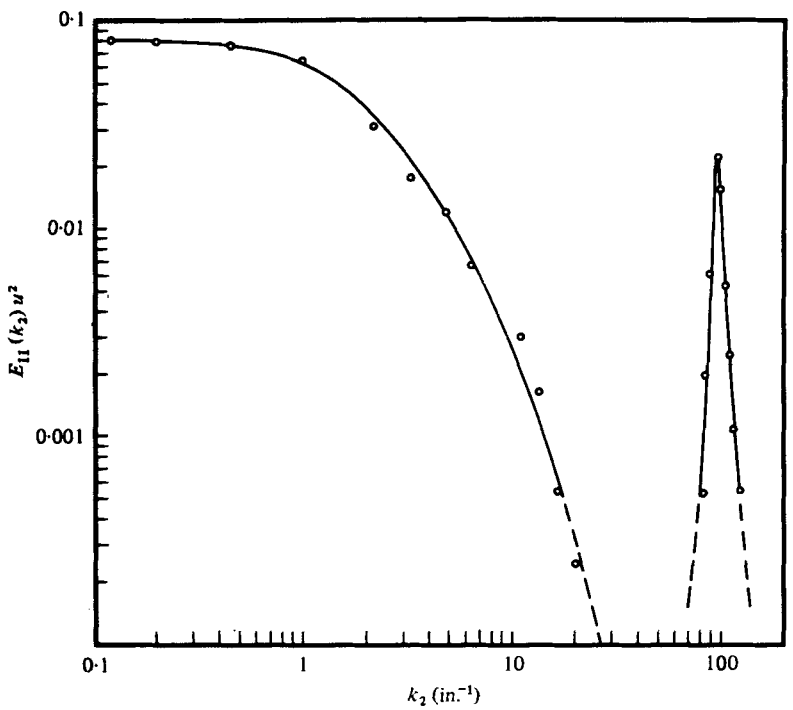

FIGURE 14. Spectrum $E_{11}(k_2)$ calculated from $R_{11}(r_2)$. $M = 2$ in.; $\Delta x_1/d = 300$.

eddy' turnover rate); u_1'/λ is proportional to the r.m.s. vorticity. α is essentially monotonic with both, but proportional to neither.

A calculation of the one-dimensional spectrum $E_{11}(k_2)$ by means of the Fourier cosine transform relation

$$E_{11}(k_2) = \frac{1}{2\pi}\int_{-\infty}^{\infty} R_{11}(r_2)\cos(k_2 r_2)\,dr_2 \tag{3}$$

was carried out on a digital computer (IBM 7094). The integral was approximated as a sum using Simpson's rule. These computations were made before the 'fast Fourier transform' came into common use.

There are three sources of error which limited the spectral resolution obtainable.

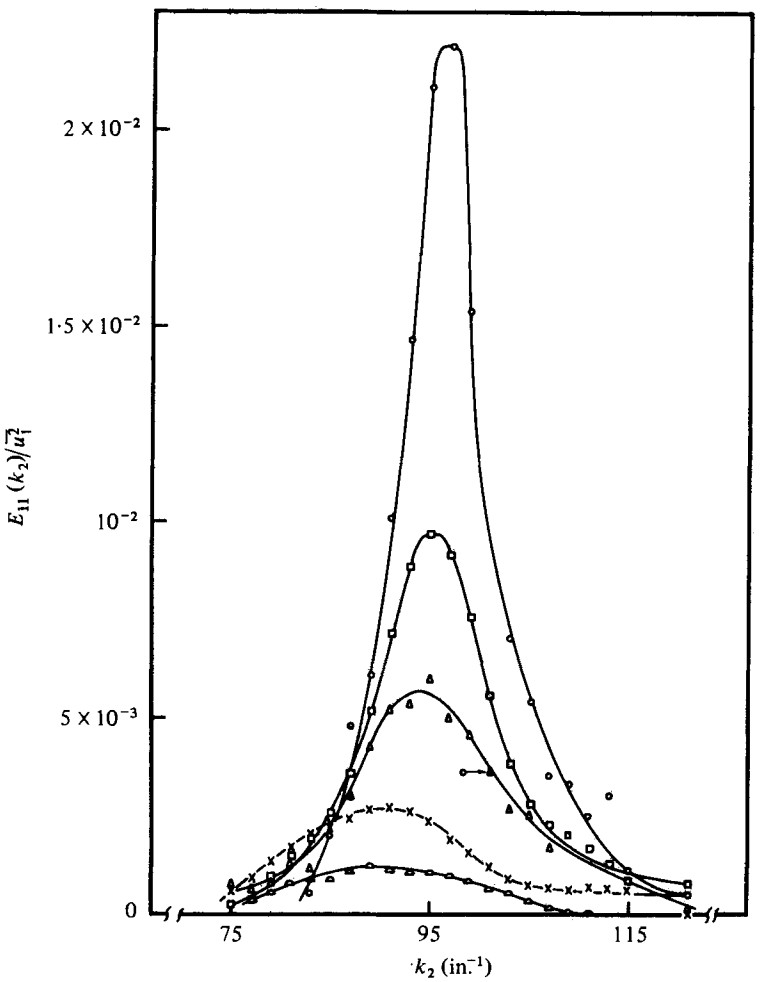

FIGURE 15. Downstream development of spectral peak in $E_{11}(k_2)$. $M = 2$ in. Values of $\Delta x_1/d$: ○, 300; □, 400; △, 500; ×, 600; ⌓, 700.

They are truncation, round-off and inaccuracies in the data. The first two were assessed by computing the transform of a function with a known transform, and then comparing the results to this known transform. With a test function $R_{11}(r_2) = (1+ar_2^2)^{-1}$, which has a decaying exponential transform, the numerical technique gave satisfactory results for $0 \leqslant k_2 \leqslant 200$ in.$^{-1}$.

There were at least two ways to use the data for this calculation. One was to substitute it directly. The other was first to plot the experimental data and then to use as 'data' for the calculation the values taken from a faired curve drawn among the data points. This latter method was used.

The results of these calculations are illustrated by figure 14, for $\Delta x_1/d = 300$, $M = 2$ in. The low wavenumber portion of this curve shows the expected monotonic decreasing character of a typical turbulence spectrum. The spectrally local chapter of the perturbation is clearly shown by the appearance of the spectral peak at

$$k_2 = 2\pi/m = 95 \text{ in.}^{-1}.$$

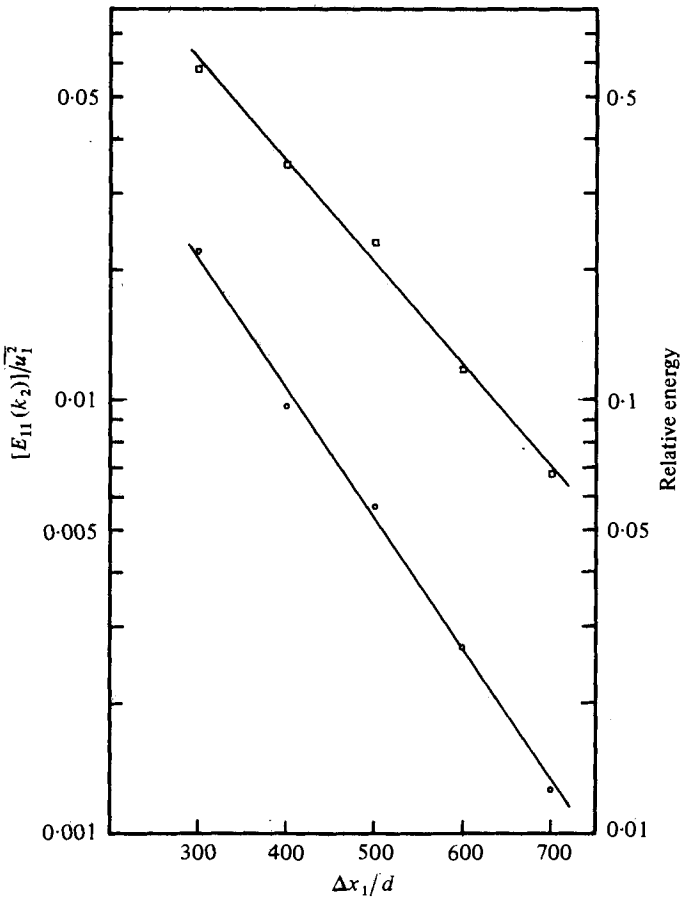

FIGURE 16. Peak values and relative energy of spectral peak in $E_{11}(k_2)$. $M = 2$ in. □, relative energy; ○, peak value.

The downstream development of this spectral peak is shown in figure 15. The computational 'noise level' indicated by dashed lines in figure 14 is attributed to inaccuracies in the data. This 'noise level' made it impossible to determine the shape of the spectral peak for $\Delta x_1/d > 800$.

Figure 16 shows a semi-log plot of the peak value and of the relative energy of the spectral peak, as functions of $\Delta x_1/d$. The relative energy was obtained by integrating the spectrum over the wavenumber range for which the spectral level was greater than 5×10^{-4}, the approximate computational noise level. The value of the integral was then normalized by dividing by the total energy.

Direct measurements of another one-dimensional spectrum, $E_{11}(k_1)$, were made in an attempt to detect an energy transfer from the wavenumber (k_2) of the perturbation to the k_1 direction. Reasoning physically in quasi-Lagrangian fashion, one might expect to detect in $E_{11}(k_1)$ a broad spectral disturbance in the range $0 < k_1 < k_2$. This would result from a rigid rotation of the periodic laminar wake structure by the random large-structure of the turbulence. To see if significant rotation can occur in

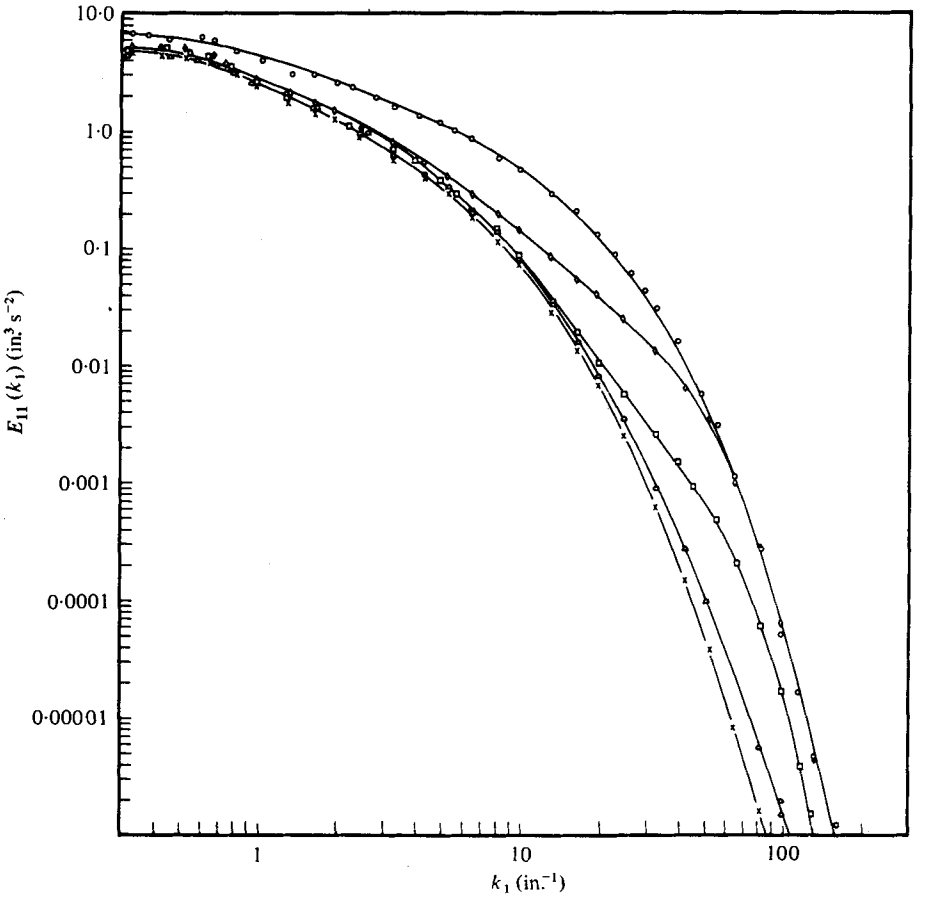

FIGURE 17. Downstream development of longitudinal spectrum $E_{11}(k_1)$ behind zither. $M = 2$ in. Values of $\Delta x_1/d$: ○, 300; ◇, 600; □, 1000; △, 1500; ×, 2000.

times comparable to the decay time of the perturbation, a comparison could be made between an inverse time constant computed from the vorticity contribution due to the turbulence spectral region at scales greater than the zither mesh size, and the inverse time constants α in (2). For simplicity, we use instead the full r.m.s. vorticity fluctuation, estimating from the exact isotropic relation

$$(\overline{\omega_i \omega_i})^{\frac{1}{2}} = \left[15 \frac{\overline{u_1^2}}{\lambda^2}\right]^{\frac{1}{2}} \tag{4}$$

(see, for example, Batchelor 1953, p. 47), we get for the (vorticity) inverse time constant $(\overline{\omega_i \omega_i})^{\frac{1}{2}} = 150\ \mathrm{s}^{-1}$. This indicates a turbulence rotation rate slower than that of the perturbation decay rate, $\alpha = 347\ \mathrm{s}^{-1}$. Viewed another way, if we use $150\ \mathrm{s}^{-1}$ as inverse time constant, and assume a rotation of $\frac{1}{2}\pi$ radians to be significant, a corresponding downstream location can be computed. The result is $\Delta x_1/d = 670$. Of course, the concomitant straining action of the turbulence on the periodic zither wake must increase the high wavenumber limit of the spectral disturbance as the flow develops. This effect is neglected in this estimate. Townsend (1951*b*) has discussed

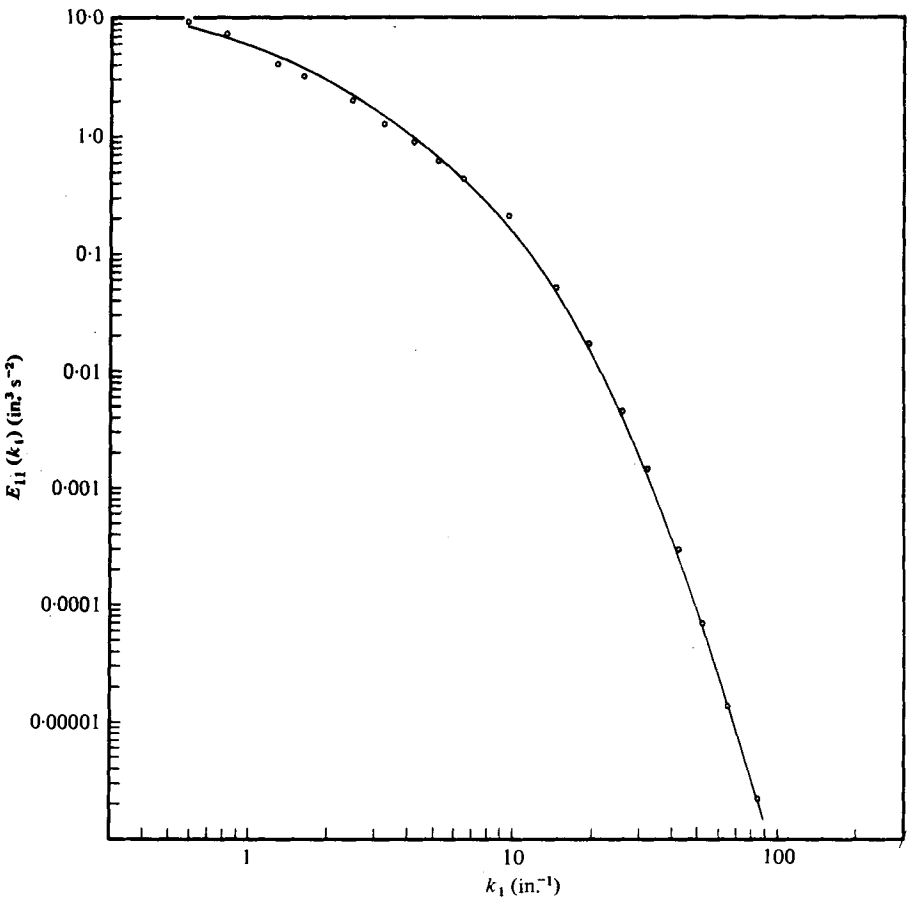

FIGURE 18. $E_{11}(k_1)$ behind grid, without zither. $M = 2$ in.; $\Delta x_1/M = 37$.

this latter phenomenon for the extremely large wavenumber (viscous) range, and Batchelor (1959) has treated the partially analogous problem for a passive scalar field being homogeneously mixed by isotropic turbulence.

Figure 17 collects the downstream development of the one-dimensional spectrum $E_{11}(k_1)$ behind the zither for $M = 2$ in., zither location $x_1/M = 37$. Figure 18 shows the one-dimensional spectrum of the undisturbed grid turbulence ($M = 2$ in.) measured at the zither location, and is included for reference. Figure 17 does show evidence of a weak, diffuse, relative spectral 'bulge' propagating towards higher wavenumbers. This impression is most pronounced at $\Delta x_1/d = 600$. This spectral evolution is in marked contrast to the decay of the one-dimensional spectrum in unperturbed grid turbulence. There the decay evolves with good similarity (see, for example, Liepmann, Laufer & Liepmann 1951; Stewart & Townsend 1951).

A measurement of the two-point velocity correlation coefficient $R_{33}(r_2)$ was also made, in an attempt to detect energy transfer from u_1 to u_3. These data were considerably less accurate than those for $R_{11}(r_2)$, partly because of the awkward problem of using two X-meters or Λ-meters, and partly because a much smaller effect was being

sought. A slight ripple in $R_{33}(r_2)$ was measured (Kellogg 1965), but this may have been a result of probe parasite sensitivity to u_1.

5. Estimate of energy amplification by the zither

As promised earlier in remarks about figures 6 and 7, we now try an estimate of the amplification of the incident turbulent kinetic energy by the low-solidity screen (the 'zither'), which was explicitly designed and operated so as to shed no von Kármán/Bénard unsteady wakes in a uniform flow. Physically, the amplification must result from the simultaneous creation of local mean shear zones by the zither wires and of turbulent ('Reynolds') shear stresses in these zones by distortion of the incident turbulence. These and other concomitant non-uniformities contribute in principle to several terms in the expression for the mean rate of production of turbulent kinetic energy, $-\overline{u_i u_k}\,\partial\overline{U}_i/\partial x_k$. Focusing our estimate on the region downstream of the zither, we suppose that: (*a*) the mean flow disturbance, the turbulent shear stress and the incremental turbulent energy can all be approximated by simple sine functions of x_2; (*b*) $-\overline{u_1 u_2}\,\partial\overline{U}_1/\partial x_2$ is the dominant production term; (*c*) the dissipation rate can be neglected for short distances behind the zither. We also neglect the energy spatial transfer, but estimate the spatial average, so this simplification is not serious. We can then make a crude and non-conservative estimate of energy amplification, using the turbulent energy equation in the vestigial form

$$\tfrac{1}{2}\overline{U}_1\frac{\partial\overline{q^2}}{\partial x_1} \approx -\overline{u_1 u_2}\frac{\partial\overline{U}_1}{\partial x_2}. \tag{5}$$

$\overline{q^2} \equiv \overline{u_k u_k}$. Instead of using a similarly stripped-down form of the shear stress equation, we simply assume that

$$-\overline{u_1 u_2} \approx 0{\cdot}5\,\overline{u^2_{1\max}}(\Delta x_1)\sin(2\pi x_2/m). \tag{6}$$

We also take $\overline{q^2} \approx 3\overline{u_1^2}$, roughly valid in a single turbulent wake. Equation (5) is then

$$\overline{U}_1\frac{\partial\overline{u_1^2}}{\partial x_1} \approx \tfrac{1}{3}\overline{u^2_{1\max}}\sin\left(\frac{2\pi x_2}{m}\right)\frac{\partial\overline{U}_1}{\partial x_2}. \tag{7}$$

$\overline{U}_1(x_1, x_2)$ and $\overline{u_1^2}(x_1, x_2)$ are then represented in the forms

$$\overline{U}_1 \approx \overline{U}\left\{1-\frac{B}{2}\cos\left(\frac{2\pi x_2}{m}\right)\exp\left(-\beta\frac{\Delta x_1}{d}\right)\right\}, \tag{8}$$

$$\overline{u_1^2} \approx (\overline{u_1^2})_0 + w(\Delta x_1)\sin^2\left(\frac{2\pi x_2}{m}\right). \tag{9}$$

$(\overline{u_1^2})_0$ is the value of $\overline{u_1^2}$ incident upon the zither, and $w(0) = 0$ is the initial condition for the differential equation. Evidently, $(\overline{u_1^2})_{\max} = (\overline{u_1^2})_0 + w$.

Substituting (8) and (9) into (7), neglecting the non-uniformity of $\overline{U}_1$ on the left side, and integrating, we get the average energy growth estimate

$$\frac{(\overline{u_1^2})_{\text{ave}}}{(\overline{u_1^2})_0} = \frac{(\overline{u_1^2})_0 + \frac{1}{2}w}{(\overline{u_1^2})_0} \approx \frac{1}{2}\left\{1+\exp\left[-\frac{\pi}{3}\frac{Bd}{m\beta}(1-e^{-\beta\Delta x_1/d})\right]\right\}. \tag{10}$$

From the measured mean velocity field, $B = 0{\cdot}25$ and $\beta = 0{\cdot}0119$. $m = 0{\cdot}064$ in. and $d = 0{\cdot}003$ in. are zither dimensions. With these values, the estimate for $\Delta x_1/d = 200$ is

$$(\overline{u_1^2})_{\text{ave}}/(\overline{u_1^2})_0 \approx 1{\cdot}8. \tag{11}$$

The measured value (figure 6) is 2·7. The considerable underestimate may be due to the failure to take account of the extremely large shears which must occur in the first few diameters behind the wires.

There is at least one other possible approach to explaining the increased u_1' levels near the zither. That is a random, lateral 'flopping' convection of the ('instantaneous laminar') periodic velocity profile past any fixed observation point by the large-scale structure of the turbulence. Experimental confirmation that this process can also account for the level changes and profiles observed is given in the appendix. The data presented there are from measurements made in the viscous wake of a cylinder oscillating in an undisturbed incident stream. To see if those results are relevant to the case of a turbulent stream incident on a fixed cylinder, a comparison of the r.m.s. oscillation amplitude with the expected r.m.s. lateral displacement of the wake due to the turbulent convection can be made. The comparison is made between data taken at $\Delta x_1/d = 300$ for the oscillating wire in a non-turbulent flow, and at $\Delta x_1/d = 100$ for the zither in turbulence. This difference in locations is used in an attempt to take into account the more rapid decay in the mean disturbance for the turbulent incident stream case. We proceed with Kampé de Fériet's (1939) form of G. I. Taylor's Lagrangian dispersion analysis,

$$X_2 = 2\overline{v_2^2}\int_0^t (t-\tau)\,R(\tau)\,d\tau, \tag{12}$$

where $R(\tau)$ is the velocity Lagrangian autocorrelation function; v_i is the Lagrangian velocity.

For small times (applicable here), $R(\tau)$ may be approximated by a parabola:

$$R(\tau) \approx 1-\tau^2/\lambda_\tau^2, \tag{13}$$

where λ_τ is the time microscale. Substitution and integration give

$$\overline{X_2^2} = \overline{v_2^2}t^2\left(1-\frac{t^2}{6\lambda_\tau^2}\right). \tag{14}$$

Scaling Kennedy's (1965) determination of λ_τ from a heat wake, and expressing t as

$$t = (\Delta x_1/d)\,(d/\overline{U}),$$

we get, for $d = 0{\cdot}003$ in., and $\overline{v_2^2} \doteq \overline{u_2^2}$,

$$\overline{X_2^2} \approx 9\left(\frac{\Delta x_1}{d}\right)^2 \frac{\overline{u_2^2}}{\overline{U}^2} \times 10^{-6}\left\{1-0{\cdot}4\left(\frac{\Delta x_1}{d}\right)^2 \times 10^{-6}\right\}. \tag{15}$$

With $\Delta x_1/d = 100$ and $u_2'/\overline{U} = 0{\cdot}02$, this gives

$$[\overline{X_2^2}]^{\frac{1}{2}} \approx 6 \times 10^{-3} \text{ in.} \tag{16}$$

The r.m.s. amplitudes of cylinder oscillation used in the work of the appendix were $9{\cdot}5 \times 10^{-3}$ in. and $4{\cdot}8 \times 10^{-3}$ in. These gave a fluctuation level comparable to the

value cited here. Thus it is plausible that this wire-wake flopping mechanism can also account for the observed increase in fluctuation levels.

From a physical point of view, we expect proper alternative explanations to be equivalent. In spatial (Eulerian) co-ordinates, the energy amplification is directly seen as the result of: (*a*) the generation of mean strain by the wire no-slip condition; (*b*) the consequent generation of off-diagonal (mean shear) terms in the Reynolds stress tensor; (*c*) the subsequent interaction of these two new attributes. The turbulent shear stress $-\overline{u_1 u_2}$, zero in the incident turbulence, is generated by the mean strain in the 'boundary layers' and wakes associated with the no-slip condition at the wire surfaces. The key term in the balance equation for $-\overline{u_1 u_2}$ is $\overline{u_2^2}\,\partial U_1/\partial x_2$. Keeping only this term, this equation in spatial co-ordinates is simply

$$\overline{U}\frac{\partial}{\partial x_1}(-\overline{u_1 u_2}) \approx \overline{u_2^2}\frac{\partial \overline{U}_1}{\partial x_2}. \tag{17}$$

A material (Lagrangian) co-ordinate description can probably be based on the view that at any instant the (distorting) 'laminar' wake of each wire is approximately a fluid material slab, and is convected downstream. The velocity non-uniformity associated with the array of flopping wakes appears as a velocity fluctuation at a fixed observation point. The lateral velocity which flops the wakes is virtually u_2, and the instantaneous local velocity gradient is approximately $\partial \overline{U}_1/\partial x_2$ near the wires. A u_1 fluctuation is thus created:

$$u_1 \sim -u_2\,\partial \overline{U}_1/\partial x_2. \tag{18}$$

Multiplying by u_2 gives the right side of (17). This explanation is much like the 'mixing length' approach of Taylor and Prandtl. Parenthetically, we note that multiplying (18) by u_1 gives the production part of the u_1 component energy equation.

6. Comparison of spectrum perturbation decay with narrow-band correlation function in unperturbed turbulence

Some years after these data were taken, Comte-Bellot & Corrsin (1971) reported measurements of narrow-spectral-band, velocity auto-correlation functions in the isotropic turbulence behind a grid nearly identical to the largest one used here. Those functions were auto-correlations in time, in a frame travelling with the mean flow. It seems plausible that, for corresponding regions of the spectrum, they should die away at about the same dimensionless rate as the narrow-spectral-band perturbations given in this report.

In order to decide which of those narrow-band correlation functions correspond to the perturbation decay functions in this study, we can compare the ratios of the characteristic wavenumber k_2, to the Kolmogorov microscale wavenumber and to the integral scale wavenumber. Somewhat arbitrarily, we may take the former as $k_\eta \equiv \eta^{-1}$ and $k_L \equiv L^{-1}$. Since $k_2 = 2\pi/m$, the last two columns in table 1 tabulate $2\pi k_L/k_2$ and $2\pi k_\eta/k_2$, respectively. Table 3 retabulates these four cases by their values of k_L/k_2 and k_η/k_2.

The corresponding ratios for the twelve narrow-band auto-correlation functions of Comte-Bellot & Corrsin are tabulated in table 4.

Comparing these pairs of ratios to those in table 3, we see that the largest wave-

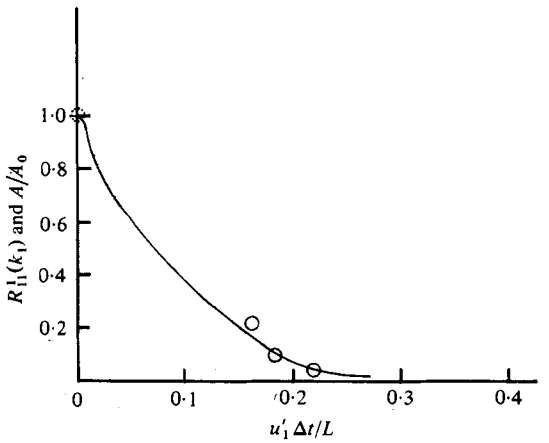

FIGURE 19. Comparison of decay of correlation function ripple to narrow-band velocity correlation function in unperturbed turbulence (Comte-Bellot & Corrsin 1971). Cases with nearly equal values of $k_{1,2}/k_L$ and $k_{1,2}/k_\eta$. ——, from Comte-Bellot & Corrsin; ○, ~ A/A_0 (present data).

Case	M = 2 in., x_1/M = 37	M = 1 in., x_1/M = 40	M = 0·5 in., x_1/M = 40	M = 1 in., x_1/M = 74
k_L/k_2	0·022	0·046	0·092	0·035
k_η/k_2	4·64	3·64	2·99	2·48

TABLE 3

k_1 (cm^{-1})	0·10	0·25	0·50	0·76	1·01	1·52	2·28	3·03	4·04	5·05	7·60	10·10
k_L/k_1	5·0	2·0	1·0	0·66	0·50	0·33	0·22	0·165	0·124	0·10	0·066	0·050
k_η/k_1	340	136	68	45	34	22	15	11	8·4	6·7	4·5	3·4

TABLE 4

number case is fairly well matched with the perturbation experiment with M = 1 in. and the zither at ${}_zx_1/M = 40$. Figure 19 is a comparison of the two functions, with $u_1'(\Delta x_1)/(L\bar{U})$ as independent variable. The agreement is surprisingly good considering that: (*a*) the amplitude of the extraneous wiggle in the perturbed correlation function is a statistical property rather different from the narrow-band correlation function of unperturbed turbulence; (*b*) the perturbation described in this report was, comparatively, not weak.

No other pairs of wavenumber ratios in tables 3 and 4 match up well but, as a matter of peripheral information, we have compared a pair for which the present experiment and the narrow-band wavenumbers of Comte-Bellot & Corrsin (1971) are in the same proportion to integral scale wavenumber, although not in the same proportion to Kolmogorov microscale. The two experiments are the M = 0·5 in. case in table 3 and the k_1 = 5·05 cm^{-1} case in table 4. Figure 20 shows that the agreement is moderately good in spite of the incomplete wavenumber match.

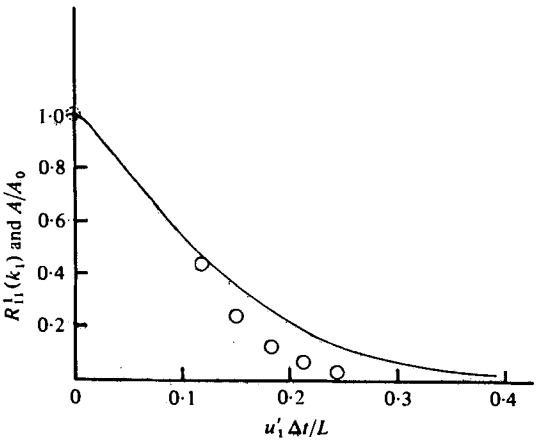

FIGURE 20. Comparison of decay of correlation function ripple to narrow-band velocity correlation function in unperturbed turbulence (Comte-Bellot & Corrsin 1971). Cases with nearly equal $k_{1,2}/k_L$, but unequal $k_{1,2}/k_\eta$. ——, from Comte-Bellot & Corrsin; ○, ~ A/A_0 (present data).

7. Comparison of spectrum perturbation decay with Kraichnan's theoretical response functions

Although it has now been recognized that Kraichnan's 'direct interaction approximation' theory (DIA) of isotropic turbulence (Kraichnan 1959; Leslie 1973*a*, cha. 5) is in part arbitrary (Kraichnan 1966; Morton & Corrsin 1970; Leslie 1973*b*), it was considerably more successful than previous theories, and it was the first one to express Fourier mode interactions in terms of an unknown 'response function', to be predicted. As mentioned in the introduction, it was a stimulus for this experiment. Unfortunately, a comparison between the measured perturbation decays, which are all for relatively large wavenumbers, and the high wavenumber form of the DIA response function is not meaningful. The reason is that the latter postulates a semicircle probability density function for velocity instead of a relatively realistic (e.g. Gaussian) one (Kraichnan, private communication). It should be mentioned that the response function decay rate of that result,

$$J_1(2u_1' k(\Delta t))]/[u_1' k(\Delta t)],$$

is comparable to the measured one.

We can, however, compare the measured data to a simpler Kraichnan prediction (1959), a *linear approximation* response function for a small perturbation at wavenumber larger than those of the initial turbulence. With the well-founded empirical Gaussian form of the velocity component probability density function (Simmons & Salter 1934; Townsend 1947) his prediction reduces to

$$\exp[-\tfrac{1}{2}\overline{u_1^2} k^2 (\Delta t)^2]. \tag{19}$$

Figure 21 compares this linear response function and with the measured decay of the amplitude of the first perturbation cycle of the correlation function $R_{11}(r_2)$, for $M = 2$ in., ${}_gx_1/M = 37$, and $M = 0{\cdot}5$ in., ${}_gx_1/M = 40$. For this comparison the time origin for the experimental perturbation decays was arbitrarily taken at $\Delta x_1/d = 300$,

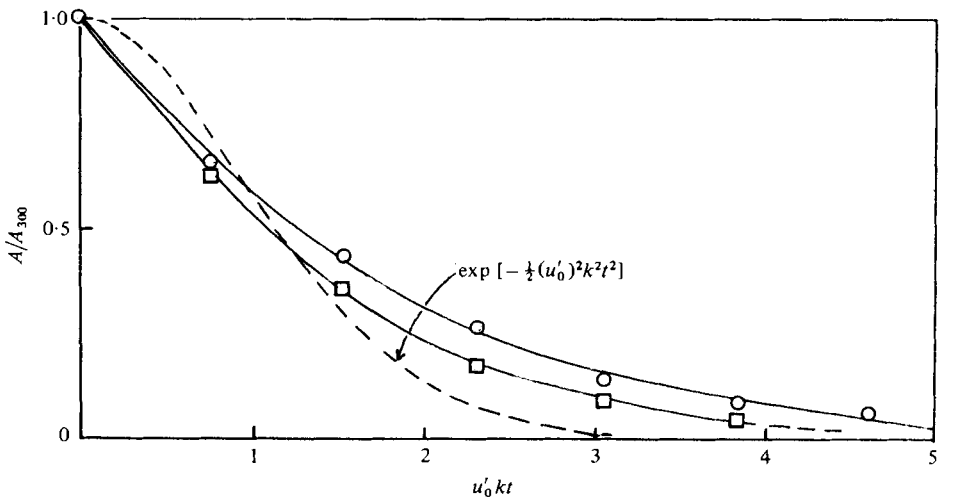

FIGURE 21. Comparison of decay of correlation function ripple with Kraichnan's linear estimate, for perturbation at relatively large wavenumber. ○, $M = 2$ in.; □, $M = 0{\cdot}5$ in.

and the amplitudes were normalized with the value there. Since the decay is closely exponential, the origin choice is not crucial.

Considering the fact that there are no arbitrary constants to scale the comparison, the agreement of Kraichnan's estimate with the experiments is remarkably good.

This paper is adapted largely from the Ph.D. thesis of R. M. Kellogg (1965). Thanks are due to the many members of the Mechanics Department who helped both directly and indirectly, in particular to D. A. Kennedy and G. Comte-Bellot for their advice and comments during the course of the work, and to M. Karweit, K. Keydel, F. Merceret and J. Shlien who helped with the data reduction and machine calculations, and to R. A. Marks for suggestions in apparatus construction. We should also like to thank the referees for their suggestions.

This work was supported in part by the National Science Foundation, through the Fluid Mechanics Program, Engineering Division, during the experimental phase of the work, and through the Meteorology Program, Atmospheric Sciences Division, during the preparation of this manuscript. R.M.K. was supported (at The Johns Hopkins University) by the International Business Machines Corporation.

Appendix. Wake behind an oscillating cylinder

A brief study of the wake behind an oscillating circular cylinder (with Reynolds number below the steady vortex-shedding range) in an undisturbed flow was undertaken to see if lateral motion of the instantaneous 'mean' speed profile past a fixed point of measurement could account for the shape of the $u_1'/\bar{U}$ profile and the increase in turbulence level observed behind the zither. As pointed out in the main text, a turbulent stream incident on a relatively thin circular cylinder operating below its vortex-shedding Reynolds number, would convect the otherwise steady laminar wake profile, thereby causing lateral displacement fluctuations. The incident turbulence

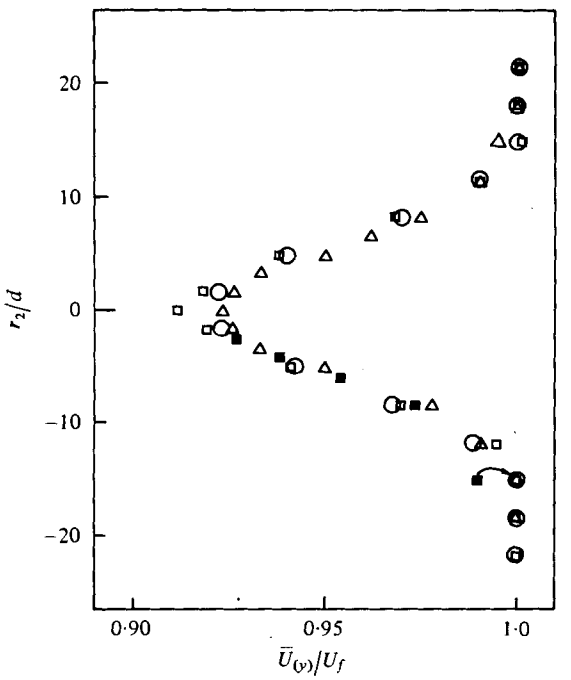

FIGURE 22. Comparison of mean velocity profiles 300 diameters behind fixed and vibrating cylinders at Reynolds number = 25, less than vortex-shedding level. Solid points (■) are *computed* by 'oscillating' the fixed wire wake (△). Peak-to-peak values of a/d, the wire oscillation amplitude: ○, 9; □, 4·5; ■, 4·5 (calculated).

would of course also strain the wake, causing its instantaneous local profile to depart from the undisturbed laminar form, but we ignore that effect in this discussion.

The approach here is to use cylinder motion to move the 'mean' profile in a known way laterally past the point of measurement, in the absence of incident turbulence. This allows clear evaluation of the effects of lateral motion of the 'mean' profile on measurements made downstream of the cylinder.

The experimental arrangement was as follows: a high carbon steel wire 0·033 in. in diameter was mounted on the wind tunnel centre-line, with its axis normal to the mean flow, in the r_3 direction. A permanent magnet gap surrounded the wire outside of the flow study segment, with the magnetic field in the direction of the mean flow. An alternating current in the wire thus produced wire oscillations in the plane normal to the mean flow. The frequency was controlled by adjusting wire tension, and the amplitude was controlled by adjusting the wire current. The wire Reynolds number was 25, and the frequency of oscillation was set at 300 Hz. The oscillation velocity added only 1% to the 'instantaneous' Reynolds number.

Figure 22 shows the mean velocity profile $\overline{U}$, and figure 23 the $u_1'/\overline{U}$ intensity profile, 300 wire diameters downstream. The profiles were measured with peak-to-peak amplitudes of wire vibration $a = 9d$ and $a = 4{\cdot}5d$. The oscillation amplitude was measured with a long focal length microscope with ruled eye-piece.

The similarity in the shape of the $u_1'/\overline{U}$ profiles obtained here to those behind the zither is evident. Furthermore, the $u_1'/\overline{U}$ levels in the wake of the oscillating wire are

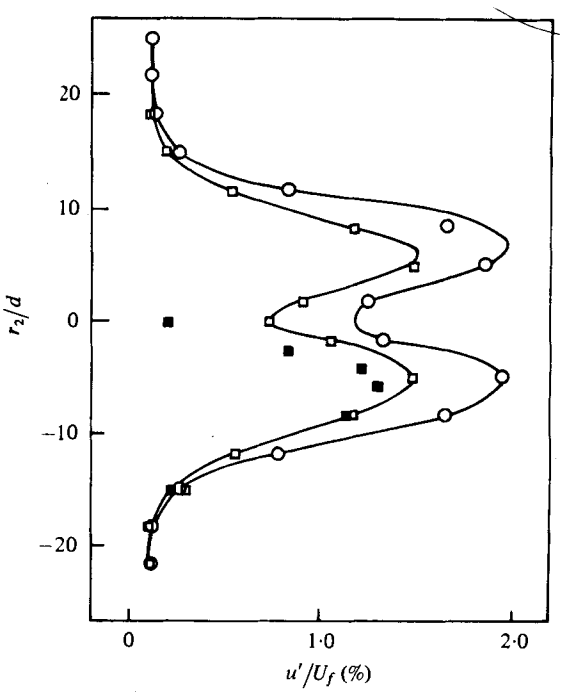

FIGURE 23. Comparison of velocity fluctuation profiles 300 diameters behind vibrating cylinder at Reynolds number = 25, less than vortex-shedding level. Solid points (■) are *computed* by 'oscillating' the fixed wire wake (△ in figure 22) with a peak-to-peak value of a/d of 4·5. Points ○ and □ are for peak-to-peak values of a/d of 9 and 4·5 respectively.

of the same order as the level changes obtained behind the zither. These facts lend support to the idea that the changes in level behind the zither can be explained in terms of turbulent lateral convection of the 'instantaneous mean wake' profile.

The mean profiles (figure 22) show remarkable similarity to each other and are not materially changed by the wire oscillation. This seems odd since one would expect the oscillation to broaden the mean profile.

A consistency check on this point, and on the $u_1'/\overline{U}$ levels as well, can be made by using the mean profile for the stationary wire case as a non-linear transfer function for an 'input' of position to an 'output' of velocity, assuming a quasi-steady flow pattern. The validity of this assumption can be checked by comparing a viscous characteristic time based on wire diameter and kinematic viscosity to the oscillation period. Taking $\tau_\nu = d^2/\nu$ as the characteristic viscous time and $\tau_0 = (2\pi f)^{-1}$ for the period of oscillation, $\tau_\nu/\tau_0 = 0{\cdot}7$. The fact that this ratio is not much less than one indicates that the assumption of quasi-steadiness is suspect.

The procedure was to obtain graphically the output velocity wave forms using a sinusoidal input of position and the non-linear transfer function based on the mean profile obtained behind a stationary cylinder. These output wave forms were calculated for different values of mean position along the transfer function. After the output velocity wave form had been obtained, its mean and mean square values were determined. These results appear as solid symbols on figures 22 and 23.

The agreement in the mean profiles indicates that the fluctuating part of the output

velocity wave form obtained graphically has a mean value close to zero. This was substantiated by observing the wave forms from the hot-wire probe on an oscilloscope. They appear closely sinusoidal over most of the range in r_2, with a doubling of frequency on the centre-line. The agreement between the computed and measured $u_1'/\overline{U}$ profile is not as close as that obtained for the mean profile. The agreement is good near the edge of the wake, worsening near the centre-line. There is, however, similarity in form and rough agreement in fluctuation level.

REFERENCES

BATCHELOR, G. K. 1953 *The Theory of Homogeneous Turbulence*. Cambridge University Press.

BATCHELOR, G. K. 1959 Small scale variations of convected quantities like temperature in turbulent fluid. Part 1. General discussion and case of small conductivity. *J. Fluid Mech.* **5**, 113–133.

COMTE-BELLOT, G. & CORRSIN, S. 1966 The use of a contraction to improve the isotropy of grid-generated turbulence. *J. Fluid Mech.* **25**, 657–682.

COMTE-BELLOT, G. & CORRSIN, S. 1971 Simple Eulerian time correlation of full- and narrow-band velocity signals in grid-generated, 'isotropic' turbulence. *J. Fluid Mech.* **48**, 273–337.

CORRSIN, S. 1959 Outline of some topics in homogeneous turbulent flow. *J. Geophys. Res.* **64**, 2134–2150.

JOHNSON, D. S. 1957 Velocity, temperature, and heat-transfer measurements in a turbulent boundary layer downstream of a stepwise discontinuity in wall temperature. *J. Applied Mech.* **24**, *Trans. A.S.M.E.* **79**, 2–8.

KAMPÉ DE FÉRIET, J. 1939 Les fonctions stationnaires et la théorie statistique de la turbulence homogène. *Ann. Soc. Sci. Bruxelles* **59**, 145–194.

KELLOGG, R. M. 1965 Evolution of a spectrally local disturbance in a grid-generated turbulent flow. Ph.D. thesis, The Johns Hopkins University.

KENNEDY, D. A. 1965 Some measurements of the dispersion of spheres in a turbulent flow. Ph.D. thesis, The Johns Hopkins University.

KRAICHNAN, R. H. 1959 The structure of isotropic turbulence at very high Reynolds numbers. *J. Fluid Mech.* **5**, 497–543.

KRAICHNAN, R. H. 1966 Invariance principles and approximation in turbulence dynamics. In *Dynamics of Fluids and Plasmas* (ed. S. I. Pai *et al.*), pp. 239–255. Academic Press.

LIEPMANN, H. W., LAUFER, J. & LIEPMANN, K. 1951 On the spectrum of isotropic turbulence. *N.A.C.A. Tech. Note* 2473.

LESLIE, D. C. 1973*a* *Developments in the Theory of Turbulence*. Clarendon.

LESLIE, D. C. 1973*b* Review of developments in turbulence theory. *Rep. Prog. Phys.* **36**, 1365–1424.

LIN, C. C. 1951 A critical discussion of similarity concepts in isotropic turbulence. *Proc. Symp. on Appl. Math. (Amer. Math. Soc.)* **4**.

MORTON, J. B. & CORRSIN, S. 1970 Consolidation expansions for estimating the response of a randomly driven nonlinear oscillator. *J. Statis. Phys.* **2**, 153–194.

ROSHKO, A. 1953 On the development of turbulent wakes from vortex streets. *N.A.C.A. Tech. Note* 2913.

SCHUBAUER, G. B. & SKRAMSTAD, H. K. 1947 Laminar boundary-layer oscillations and transition on a flat plate. *J. Res. Nat. Bureau of Standards* **38**, 251–292.

SCHUBAUER, G. B., SPANGENBERG, W. G. & KLEBANOFF, P. S. 1950 Aerodynamic characteristics of damping screens. *N.A.C.A. Tech. Note* 2001.

SIMMONS, L. F. G. & SALTER, C. 1934 Experimental investigation and analysis of the velocity variation in turbulent flow. *Proc. Roy. Soc.* A **145**, 212–234.

STEWART, R. W. 1952 An experimental study of homogeneous and isotropic turbulence. Ph.D. thesis, University of Cambridge.

STEWART, R. W. & TOWNSEND, A. A. 1951 Similarity and self-preservation in isotropic turbulence. *Phil. Trans. Roy. Soc.* A **243**, 359–386.

TOWNSEND, A. A. 1947 The measurement of double and triple correlation derivatives in isotropic turbulence. *Proc. Camb. Phil. Soc.* **43**, 560–570.

TOWNSEND, A. A. 1949 Fully developed turbulent wake of a circular cylinder. *Austr. J. Sci. Res.* A **2**, 451–468.

TOWNSEND, A. A. 1951*a* The passage of turbulence through wire gauzes. *Quart. J. Mech. Appl. Math.* **4**, 308–320.

TOWNSEND, A. A. 1951*b* On the fine-scale structure of turbulence. *Proc. Roy. Soc.* A **208**, 534–542.

TOWNSEND, A. A. 1956 *The Structure of Turbulent Shear Flow.* Cambridge University Press.

UBEROI, M. S. & CORRSIN, S. 1953 Diffusion of heat from a line source in isotropic turbulence. *N.A.C.A. Rep.* 1142.

WISKIND, H. K. 1962 A uniform gradient turbulent transport experiment. *J. Geophys. Res.* **67**, 3033–3048.